[Frontiers in Bioscience, Landmark, 20, 1079-1091, June 1, 2015]

A Monte Carlo simulation dissecting quantal release at the calyx of Held

Jun Guo[1], Zhi-cheng Sun[1], Pan-tong Yao[1], Hong-li Wang[1], Lei Xue[1]

[1]Department of Physiology and Biophysics, School of Life Sciences, Fudan University, Shanghai, P.R. China, 200438

TABLE OF CONTENTS

1. ABSTRACT

Although quantal release provides a basic control of synaptic strength, its underlying mechanisms remain unclear. Here, we report a refined realistic 3D vesicle fusion model at calyx-type synapses. By refining the micro ultrastructure and combining updated parameters, our model is appropriate for simulating quantal release. First, we confirmed the existence of kiss-and-run fusion and gave a justified estimation of its percentage in spontaneous and stimulated release. Second, we found the location of AMPA receptors caused the huge variation in the mEPSC rise time. Third, glutamate spillover only slightly contributed to the mEPSC decay time in small vesicles but caused a dual-peak event in large vesicles. Fourth, mEPSC rise time increased with amplitude, suggesting the contribution of vesicle size, not glutamate concentration. We also applied our model to the analysis of KCl, $CaCl_2$ and synaptotagmin-2 triggered exocytosis. KCl globally accelerated the mEPSCs, whereas mEPSCs were slowed down in high calcium treatments and synaptotagmin-2 knock-out mice, indicating more kiss-and-run release. In summary, our model provides a convenient method for exploring the detailed mechanism of vesicle fusion.

2. INTRODUCTION

Synaptic transmission plays a critical role in communication between neurons and is determined by quantal release of neurotransmitter (1, 2). During exocytosis, synaptic vesicles filled with neurotransmitter fuse with presynaptic nerve terminals via different fusion modes, and the released neurotransmitter diffuses across the synaptic cleft, finally binding to the postsynaptic receptors to generate the excitatory/inhibitory postsynaptic response. Several parameters have been suggested to critically affect synaptic strength: 1) neurotransmitter concentration within synaptic vesicles and its diffusion rate after fusion (3, 4), 2) the vesicle fusion mode, such as kiss-and-run (5-8), full collapse fusion (8-10), or multi-vesicular release (11, 12), and 3) the properties of postsynaptic receptor cluster, such as its density and location (3). The amount of neurotransmitter available provides the basic supply for quantal release, and the diffusion rate critically influences the amplitude and latency of the postsynaptic response. However, accurate measurements have been proved to be a challenging task due to technical difficulty. In Drosophila, a glutamate concentration of 407 mM has been reported (13), which corresponds to 16000 glutamate molecules within a vesicle with a diameter of 46 nm (14). In the mammalian cortex, several pioneer studies have provided some ballpark estimations of N_{glu}, which ranges from 2000 to 6000 of glutamate depending on the protocol (15-18). Due to a lack of accurate inner volume information for synaptic vesicles after chemical fixation for tissue preparation, the value of N_{glu} may be underestimated. A recent study reported a N_{glu} value of 5000 - 9000 with a corresponding diffusion rate

(D_{glu}, 0.2. - 0.4. $\mu m^2.ms^{-1}$) that could match the real mEPSC recordings (4). However, a simple analytical diffusion equation was applied to estimate the glutamate concentration in the synaptic cleft after exocytosis, ignoring the complicated parameters during exocytosis, such as fusion pore opening and dilation, vesicle size variation, binding of transmitter to the receptors and transmitter crosstalk. Therefore, the N_{glu} could still be underestimated. In addition, the vesicle fusion mode has been suggested to control both the amount and speed of neurotransmitter release, determining the synaptic strength and plasticity (7, 8, 11). A previous simulation was proposed to show the different postsynaptic kinetics between full fusion and kiss-and-run at the calyx of Held (8). However, this model still has caveats and needs to be improved. For example, the 2 nm pre- and post-synaptic barriers in the model do not exist. Also, the parameters used in the model are from different preparations and the binding reactions of glutamate to AMPA receptors are from cerebellar Purkinje cells, which should not be combined together to mimic the real kinetics of synaptic transmission at calyx-type synapses. Furthermore, the density and location of postsynaptic AMPA receptors are also involved in controlling synaptic strength. The postsynaptic receptor cluster size and its relative distance from the release site affect the amplitude and speed of the postsynaptic current (19, 20). Neurotransmitter spillover has also been reported to contribute to the shape of the postsynaptic currents in several synapses (21-24).

Although all of the parameters mentioned above are crucial to understanding the detailed kinetics of synaptic transmission, precise measurements are quite difficult and progress very limited. Here, we report a Monte Carlo simulation (MCell, version 3.2.1.) of single vesicle fusion at calyces synapses to help understand the variation in quantal release (25). We applied a more realistic cellular ultrastructure with updated parameters and found a combination of N_{glu} and D_{glu} (10000, 0.2.5) that was a better match of the real postsynaptic recordings. When comparing the simulation results with real recordings, we found that 1) the kiss-and-run mode of vesicle fusion exists and its percentage could be roughly estimated by our model, 2) the distance between AMPA receptor cluster and release site is the major cause of variations in the mEPSC rise time, 3) transmitter spillover plays only a minor role in small vesicles while causing a dual-peak in large ones, 4) vesicle size, not glutamate concentration inside vesicles, causes the increase in mEPSC amplitude and rise time.

3. MATERIALS AND METHODS

3.1. Electrophysiology

Postnatal day 7-10 (p7 - p10) old Sprague Dawley (SD) rats of either sex were decapitated and the brain stems containing the medial nucleus of the trapezoid body (MNTB) were quickly moved to a chamber filled with iced artificial cerebral spinal fluid (ACSF) containing (in mM): 125 NaCl, 2.5. KCl, 25 NaHCO3, 3 *myo*-inostol, 2 Na-pyruvate, 1.2.5 NaH2PO4, 0.4. ascorbic acid, 25 D-glucose, 1 MgCl2, and 0.0.5 $CaCl_2$, at pH 7.4. when bubbled with 95% O_2 and 5% CO_2. Parasagittal brainstem slices (200 μm thick) were prepared using a vibratome (VT 1200s, Leica, Germany). The slices were incubated for 30 min at 37°C and then held at room temperature (22 - 24°C) for experiments. For postsynaptic recordings, the bath solution contained (in mM): 125 NaCl, 2.5. KCl, 25 NaHCO3, 3 *myo*-inostol, 2 Na-pyruvate, 1.2.5 NaH2PO4, 0.4. ascorbic acid, 25 D-glucose, 1 MgCl2, 2 $CaCl_2$, and 0.0.01 TTX, at pH 7.4. when bubbled with 95% O_2 and 5% CO_2. The postsynaptic pipette (2 - 3 MΩ) solution contained (in mM): 125 K-gluconate, 20 KCl, 4 Mg-ATP, 10 Na_2-phosphocreatine, 0.3. GTP, 10 HEPES, and 0.5. EGTA, pH 7.2., adjusted with KOH (osmolarity 310 - 320 Osm). To isolate AMPA receptor-mediated mEPSCs, blockers of NMDA receptors (D-APV, 50 μM), $GABA_A$ receptors (bicuculline, 10 μM) and glycine receptors (strychnine, 10 μM) were also added to the bath solution. Whole-cell postsynaptic mEPSC events were collected using patch master software (version 2.7.3) with EPC-10 amplifier (HEKA, Lambrecht, Germany) with Rs compensation of 90% unless otherwise noted. The synaptotagmin-2 (*syt2*) knock-out mice were bred using standard mouse husbandry procedures (11, 26). In *syt2* knockout, part of exon 2 through exon 7 was replaced by a lacZ cassette (26, 27). Genotyping was performed by PCR and confirmed by immunoblotting. The mEPSCs of wild-type and knock-out mice were recorded without Rs compensation to decrease the baseline noise and detect more events. If not mentioned, the statistical analysis was t-test and means are presented as ± SE. All animal protocols followed the guidelines approved by the Animal Care and Use Committee of Fudan University.

3.2. Electron microscopy (EM)

EM procedures were similar as described before (11). Briefly, serial ultra-thin sections (~90 nm in thickness) through the MNTB were used to measure vesicle size. These sections were viewed and photographed with a CCD digital camera system. EM images were photographed at a primary magnification of 10,000X and saved as a zero loss file format (TIFF).

As the shape of some vesicles is slightly elliptical, vesicle diameters were measured for perpendicularly oriented long (a1) and short (b1) axes between the outsides of the outer leaflets, and between the insides of the inner leaflets (a2, b2). The mean diameter (d) was approximated by d=((a1*b1*c1)1/3 + (a2*b2*c2)1/3))/2, where c1 = (a1 + b1)/2, and c2= (a2+ b2)/2 (28).

3.3. Simulation

We performed simulations of quantal release at the calyx of Held with MCell (version 3.2.1.), a modeling tool based on the Monte Carlo algorithm that simulated

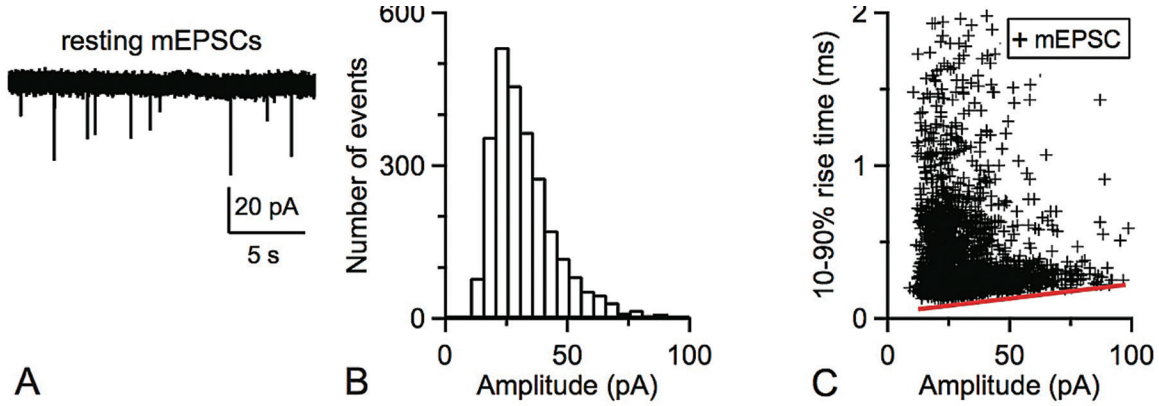

Figure 1. Postsynaptic mEPSC recordings at calyx of Held. (A) Sampled mEPSCs in the resting condition. (B) The amplitude distribution of mEPSCs. The mean amplitude was 32.0. ± 0.3. pA (n = 2643). (C) Scatter plot of 10-90% rise time versus mEPSC amplitudes. The red line shows the fitting of rise time increased with amplitudes.

the stochastic behavior of molecule diffusion in complex micro-environment. All of the simulations were run on the Fudan University computer cluster, which is a parallel processing system running a Linux operation system. Briefly, the pre- and post-synaptic membranes were represented by two paralleled 2 μm x 2 μm planar sheets, with a 28 nm (14) synaptic cleft between the sheets. The area of pre- and post-synaptic membranes was large enough for our simulations because further enlargement of the area would not cause discernible change in simulation output. The synaptic vesicle was simulated as a cube with an inner edge length of 37 nm that had the equivalent volume of a sphere with a diameter of 47 nm, the average diameter of vesicles at the calyx of Held based on our EM data (also see (14)). The number of glutamate molecules (N_{glu}) in the cube was set to 10000. The center of the cube was placed 33.5. nm above the center of the presynaptic sheet so that the bottom face of the cube could be connected to the presynaptic sheet with a fusion pore of 15 nm length (8, 29). Sixty AMPA receptors were scattered in a 0.0.5 μm^2 area (0.2.24 μm * 0.2.24 μm), which corresponded to the average area of a postsynaptic receptor cluster at the calyx of Held (4). The number of AMPA receptors was within the range of 40 to 70 based on two previous EM experiments (variation from 40 - 70 has been attempted and we chose 60 because it matched our recordings best, see Figure 2A, (4, 14)). The AMPA reaction scheme was taken from a previous study (4) in which the AMPA kinetics were measured at the calyx of Held using an outside-out patch clamp technique. A range of 0.2. - 0.4. $\mu m^2 . ms^{-1}$ has been reported for the glutamate diffusion coefficient (30), so we chose a combination of N_{glu} and D_{glu} (10000, 0.2.5) that would best match the mEPSCs collected in this study. Several other possible pairs within the range ($5000 < N_{glu} < 80000$, $0.2. < D_{glu} < 0.4.$) have also been tested (data not shown (30, 31)). The final simulated response was averaged from 50 runs with random seeds.

To mimic different vesicle fusion modes, we set the initial fusion pore size to 1.1. nm, 2.3. nm and 6 nm in different simulations, corresponding to pore conductances (G_p) of 66 pS, 288 pS and ∞ respectively, based on a previous report using a cell-attached patch clamp configuration (see Equation 1 below, (8)).

$$D_p=(4*G_p*\rho*\lambda/\pi)^{0.5.} \quad (1)$$

where ρ is the saline resistivity (100 .cm) and λ is the fusion pore length (15nm).

We also varied the distance between the postsynaptic receptor cluster and the release site (0 nm - 1500 nm, measured at the postsynaptic membrane) to simulate release at different locations. To evaluate the contributions of vesicle size and postsynaptic receptor density, different cube size (inner edge length 19 - 61 nm) and different numbers of AMPA receptors (40 - 100) have also been tested. The AMPA receptor reaction scheme used in the previous study was obtained in cerebellar Purkinje cells which may not be suitable for simulations at the calyx of Held (8). Our model was based on an updated reaction scheme from a recent study at the calyx of Held (4).

4. RESULTS

4.1. Large variation in mEPSC rise time

To better simulate single vesicle fusion kinetics, mEPSCs were collected from principal neurons at the calyx of Held. All recordings were performed with a whole-cell configuration at a resting potential of -80 mV and 1 μM TTX to block action potential firing. We collected 2643 mEPSC events in total. The mean amplitude was 32.0. ± 0.3. pA and the mean frequency 1.1. ± 0.1. Hz (n = 12, Figures. 1A, B). The histogram of mEPSC amplitudes and distribution of 10-90% rise time were plotted in Figures. 1B and 1C. The rise time distribution

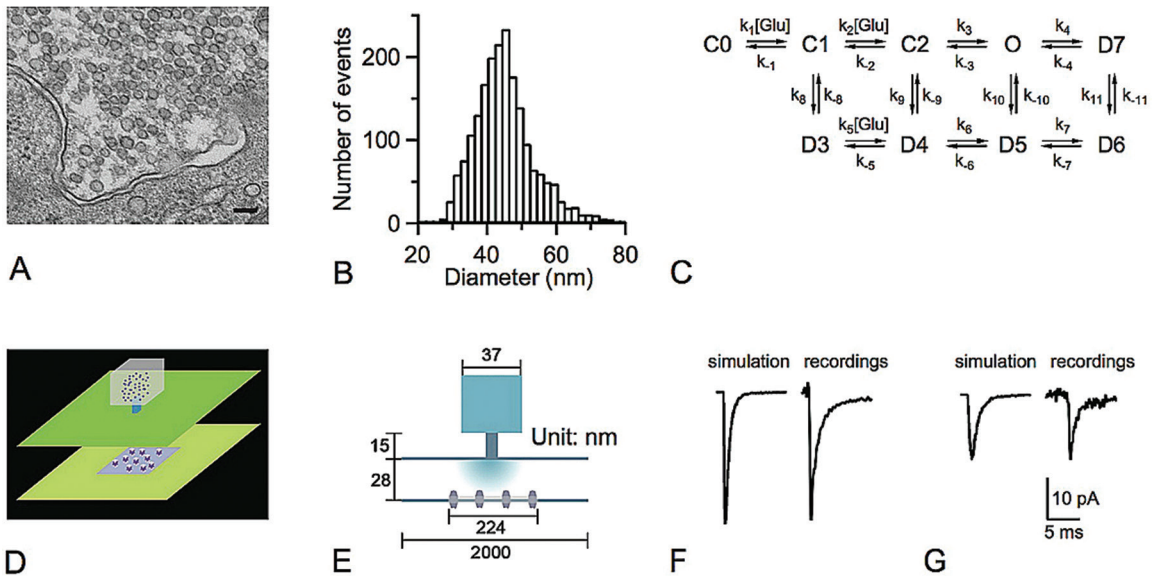

Figure 2. Monte Carlo simulation of quantal release. (A) EM image of rat calyx of Held (scale bar: 100 nm) in the resting condition. (B) Distribution of vesicle diameter at the calyx of Held (n = 2039 from 4 rats). (C) AMPA receptor reaction scheme from calyx-type synapses. (Rates: k1 = 1.8.412x10^7, k-1 = 4.3.23x10^3, k2 = 4x10^6, k-2 = 1.7.201x10^4, k3 = 5.1.69x10^4, k-3 = 1.0.082x10^4, k4 = 1.3.80x10^3, k-4 = 421.8.49, k5 = 1.9.863x10^7, k-5 = 1.1.68x10^3, k6 = 848.1.41, k-6 = 538.9.20, k7 = 51.7., k-7 = 29.1.64, k8 = 885.9.90, k-8 = 280.3.5, k9 = 449.0.33, k-9 = 1.9.44, k10 = 2.7.97, k-10 = 39.4.97, k11 = 939, k-11 = 24.4.63. Unit: M−1•s−1 for k1, k2, k5 and s-1 for the rest.) (D) 3D model synapse at the calyx of Held. Vesicle filled with neurotransmitters, fusion pore, pre- and post- synaptic membrane and the postsynaptic AMPA receptor cluster are shown in different colors. (E) 2D cartoon of quantal release. The vesicle size, fusion pore, synaptic cleft, and postsynaptic AMPA cluster are labeled. (F) Left: simulated mEPSC of full fusion in a 47 nm vesicle with Gp >375 pS. Right: averaged traces from recordings of fast mEPSCs. (G) Left: simulated mEPSC of kiss-and-run fusion in a 47 nm vesicle with Gp of 288 pS. Right: averaged traces from recordings of slow mEPSCs.

was quite scattered, and two major observations can be made. First, the 10-90% rise time varied dramatically against amplitude; for example, a similar amplitude of 40 pA could have a rise time of 0.1.4 to ~2 ms. Second, at the fastest rise time (red line, Figure 1C), the rise time slightly increased with amplitude. For example, the fastest rise time at 40 pA was 0.1.4 ms, at 80 pA was 0.1.8 ms, and at 120 pA the rise time further increased to 0.2.1 ms. This increase in rise time against amplitude at the bottom of the scatter plot could be fitted by a linear fitting with a slope of 1.7. μs.pA^{-1} (red line, Figure 1C).

A previous model of vesicle fusion showed that kiss-and-run fusion has a slower rise time than full collapse fusion (8). However, the scattered distribution of rise time could not be fully explained by the difference in fusion modes. We set up a 3D realistic model in MCell to simulate real molecules diffusion and reactions in the micro-environment (Figures. 2D, E, see Methods for details). We used this model to generate the postsynaptic current that could be compared with mEPSCs from recordings. The AMPA receptors being activated during simulation could mirror the response of mEPSCs (3). Our EM results showed that vesicle sizes at the calyces were within the range of 24 to 76 nm with a mean value of 47.1. ± 0.4. nm (n = 2039 from 4 cells, Figures. 2A, B), which is consistent with a previous study (14). The AMPA receptor reaction scheme (Figure 2C) was from a recent study at the calyx of Held (4).With the variation of N_{glu} from 5000 to 16000 and D_{glu} from 0.2. to 0.4. $\mu m^2.ms^{-1}$, we chose a pair (10000, 0.2.5) that would best fit our mEPSC recordings. First, we simulated single vesicle fusion with full fusion mode (initial fusion pore conductance >375 pS) and the postsynaptic receptors were aligned directly opposed to the release site (8). The simulation of mEPSC was averaged from 50 runs with different random seeds, and the corresponding current of the simulated mEPSC could be calculated as $N_{AMPA\_open} * V_{hold} * g_{AMPA}$, where N_{AMPA_open} was the number of activated channels, g_{AMPA} was the average conductance of AMPA receptors (20 pS) (32), and V_{hold} was the holding potential, -80 mV. Fig 2F (left) shows the averaged simulated mEPSC of 31.8. pA with 10-90% rise time of 0.1.5 ms. The averaged trace from fastest mEPSCs in real recordings is shown in Figure 2F (right) for comparison. Second, we simulated the quantal release with kiss-and-run fusion. When a Gp of 288 pS was chosen (8), which corresponded to an initial fusion pore of 2.3. nm, the amplitude of the simulated mEPSC was 15.5. pA with 10-90% rise time of 0.5.0 ms (Figure 2G, left). Similar events could also be found in real recordings (Figure 2G, right).

4.2. Evaluation of kiss-and-run in resting and KCl stimulated condition

The diversity of rise time has been reported to be caused by different vesicle fusion modes (8). To

obtain a rough estimation of the ratio of kiss-and-run events, we chose the maximum Gp (288 pS) that can be detected by cell-attached recording (8) as the threshold and combined simulation results from the smallest and largest vesicles (~24 and ~76 nm in diameter from our EM measurements, Figure 2B) to set the criteria for kiss-and-run events. The simulated amplitude of the largest vesicle 76 nm in diameter (20 pA) and rise time of the smallest vesicles of 24 nm in diameter (0.2.2 ms) were used as the upper amplitude and lower rise time thresholds for selecting kiss-and-run events. A decrease in Gp and change in vesicle size from 24 to 76 nm would result in the combination of amplitude and rise time to be <20 pA and >0.2.2 ms. In our 2643 mEPSC events, 327 events (12.4.%) fell in this range, suggesting the proportion of kiss-and-run fusion with fusion pore size under 288 pS at resting condition (8). Notably, this value was still underestimated because some events with small Gp in resting condition had very small amplitudes that could not be detected. Also, we could not rule out the possible contribution of postsynaptic location. However, most AMPA receptors are scattered in an area of 0.0.5 μm^2 directly opposite the release site, where a majority of the mEPSCs would not fall into the kiss-and-run range.

Does kiss-and-run fusion remain the same in the stimulated condition? To test this idea, we compared new mEPSCs collected from resting and KCl (50 mM) stimulated conditions. A total of 750 events from the resting group (n = 5) and 671 events from the stimulated group (n= 4) are shown in Figure 3. The amplitude distribution shifted to the right, which reflects the increase of mEPSC amplitudes during KCl stimulation (resting: 32.0. ± 1.4. pA; stimulation: 52.6. ± 7.6. pA, Figure 3B). This result was consistent with our previous report (11). However, the scatter plot of rise time versus amplitudes moved downwards (Figure 3C) and the cumulative probability curve shifted to the left compared to the resting condition ($p < 0.0.01$, K-S test), which suggests accelerated vesicle fusion (Figure 3D). Based on the same criteria mentioned above, the kiss-and-run fusion occupied 3.6.% of the total events, which was less than in the resting condition (12.4.%). KCl stimulation not only increased the frequency of transient fusion events caused by kiss-and-run, but also increased the fusion pore opening rate (most of them are >288 pS, which could not be detected in cell-attached recordings) and decreased the faction of events with slowest fusion pore opening (8, 33). Our estimation in the KCl stimulation was very close to the previously reported value from cell-attached recordings, which indicated that only 3% of all fusion events were kiss-and-run with a pore size under 288 pS (8).

4.3. Location of postsynaptic receptor cluster determines the variation in mEPSC rise time

The widely scattered distribution of 10-90% rise time in Figure 1C was not fully explained by full fusion and kiss-and-run. Two other mechanisms are possible: 1) the distance of the postsynaptic receptor cluster to the release site and 2) the glutamate concentration within the vesicles. Our model confirmed the first mechanism. We varied the distance between the center of the AMPA receptor cluster and the release site from 0 to 1500 nm in our model (Figures. 4A, B), which covered most variation of the distance (4), and found that the simulated mEPSC had a decreased amplitude with slower 10 -90% rise time (amplitude: 32 - 0.9.6 pA, rise time : 0.1.5 - 0.4.7 ms, Figure 4C). The simulated responses shown in Figure 4C were from distances between 0 and 800 nm because further increases in distance resulted in very low amplitude and the rise time was hard to measure. The simulation results matched our recordings and provided a reasonable explanation for the variation in rise time.

The glutamate concentration inside vesicles ($(Glu)_v$) critically determines variations in quantal size and rise time (3). To further clarify whether an increase in rise time with amplitude is caused by glutamate concentration variation, we recorded mEPSCs by glutamate dialysis with another pipette containing 100 mM glutamate positioned at the presynaptic terminal in whole-cell configuration (3, 34). Within 10 s after break-in and dialysis of glutamate, the mEPSC amplitudes increased (Figure 4D). The 10-90% rise times of mEPSCs were plotted against amplitudes from two groups in Figure 4E. Obviously, the mEPSCs in the 100 mM glutamate group had smaller rise times than those in the control group, indicating that increased $(Glu)_v$ decreased the rise time. Our simulation also confirmed these results (Figure 4F). We used various glutamate concentrations up to 35000 molecules per vesicle in our model and found that the 10-90% rise time decreased as amplitude increased.

4.4. Increase of vesicle size causes larger mEPSC with slower rise time

The other observation in Figure 1C was the slight increase in rise time with increasing mEPSC amplitudes at the bottom of the scattered distribution (red line). In general, the events on the red line reflected full collapse fusion at the closest distance to the release site. The increase in 10-90% rise time could not be attributed to the increase in glutamate concentration. As shown above, the rise time would decrease if the amplitude increase was caused by an increase in glutamate concentration. Another possibility that could account for amplitude increase is vesicle size variation. A linear relationship between quantal size and vesicle volume has been reported in Drosophila synapses (13). We also observed variation in vesicle size at the calyx of Held (Figures. 2A, B). If the large vesicle size was the cause of the amplitude increase, it would predict a slower rise time (11). We tested this idea in our model with different vesicle sizes of 24 to 76 nm (Figure 4G). The simulation results clearly show that larger vesicles had slower 10-90% rise times (increase from 0.1.0 ms in 24 nm vesicles to 0.1.7 ms in 76 nm vesicles, Figure 4H).

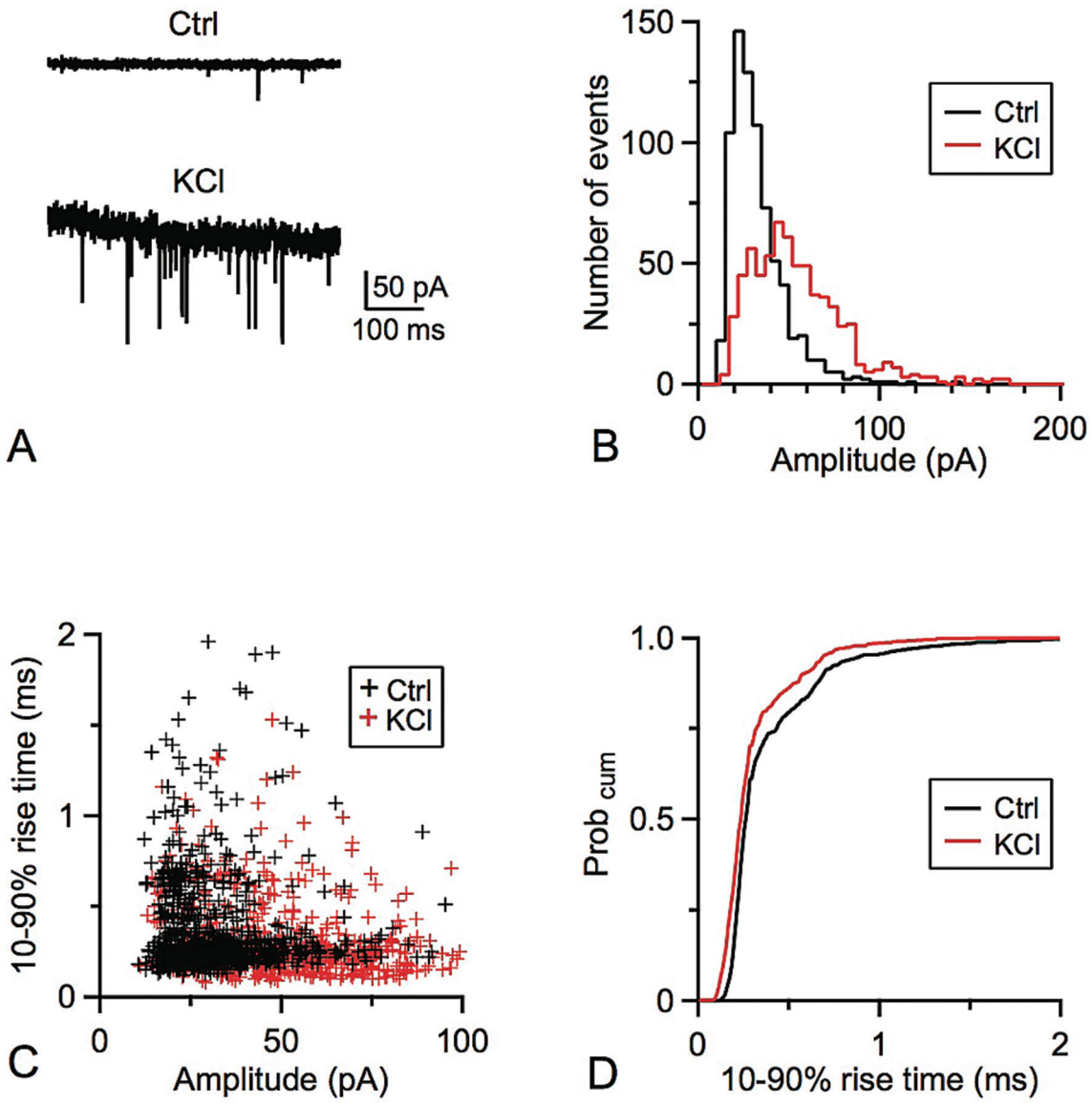

Figure 3. KCl stimulated acceleration of quantal release. (A) Sampled mEPSC recordings in control (upper) and during KCl application (lower). (B) The amplitude distribution of mEPSCs in control (black) and KCl stimulation (red). Control: 750 events with mean amplitude of 32.0. ± 1.4. pA (n = 5); KCl: 671 events with mean amplitude of 52.6. ± 7.6. pA. (C) Scatter plot of rise time versus amplitudes of control (black) and KCl stimulation (red). Events in KCl stimulation exhibited a downward distribution of 10-90% rise time against amplitudes. (D) Cumulative probability curve of rise time for control (black) and KCl stimulation (red). The red curve shifted to the left, suggesting an acceleration of quantal release during KCl stimulation.

4.5. Evaluation of neurotransmitter spillover with different vesicle size

Neurotransmitter spillover has been reported to enhance transmission in some preparations (21, 35), but whether it also contributes to resting spontaneous release is unclear. A previous report showed a minor effect of transmitter spillover at the end of the decay phase of simulated mEPSC (4). However, this result only included a response from a single surrounding receptor cluster and did not take vesicle size variation into account. We further tested this idea with different vesicle size. We mimicked the spillover effect by adding another AMPA receptor cluster 800 nm from the release site, which reflected the average distance between two postsynaptic clusters (Figure 5A). Because spillover could occur from all four surrounding directions, the final response was enlarged four-fold before adding up to the non-spillover mEPSC response (Figures. 5A, B). Our simulation results show that, for small vesicles ~24 nm in size, the spillover of glutamate did not affect the amplitude or 10-90% rise time, and it only slightly

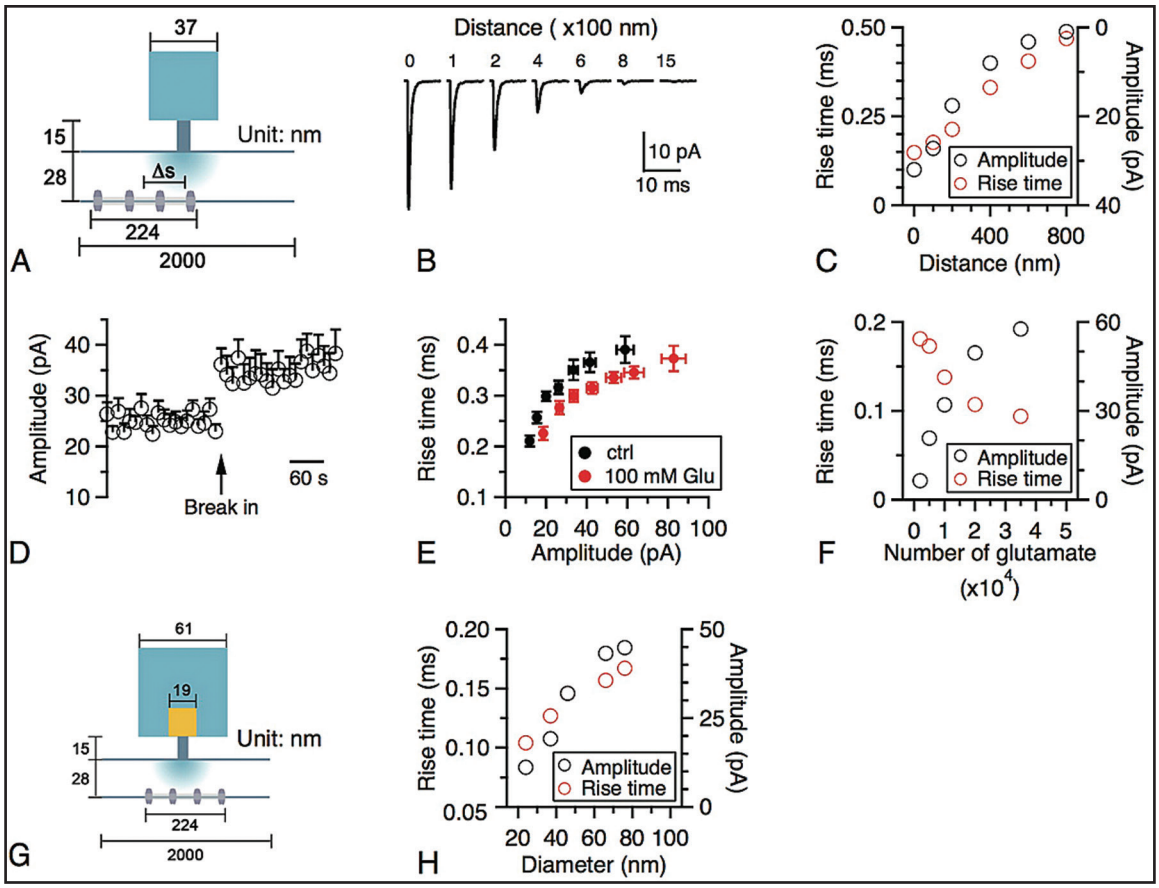

Figure 4. The location of the AMPA receptor cluster and vesicle size contribute to the variation in mEPSC rise time. (A) 2D cartoon of quantal release showing different locations of the AMPA receptor cluster at the postsynaptic membrane. Δs is the distance between the center of the AMPA receptor cluster and the release site. (B) Simulated mEPSC with different Δs ranging from 0 to 1500 nm. (C) Plot of 10-90% rise time (red circle) and amplitude (black circle) of simulated mEPSC versus Δs. The rise time increases with distance, whereas amplitude decreases with distance. (D) The average mEPSC amplitude (binned every 10s) plotted against the time after presynaptic whole-cell break in (arrow) with a pipette containing 100 mM glutamate (n = 4). (E) The 10-90% rise time versus amplitudes in control (n = 4, black) and 100 mM glutamate groups (n = 4, red). The mEPSCs in the 100 mM glutamate group had a faster rise time at all amplitudes. (F) Simulation of (Glu)v variation showing that increased (Glu)v increases mEPSC amplitude (black circle) and decreases the 10-90% rise time (red circle). (G) 2D cartoon showing the variation in vesicle size at calyces: 24 nm and 76 nm diameter vesicles are shown with edge lengths of 19 nm and 61 nm. (H) Plot of 10-90% rise time (red circle) and amplitude (black circle) of simulated mEPSCs versus vesicle diameter with constant glutamate concentration. The rise time and amplitude both increase with vesicle diameter.

contributed to the decay of the mEPSC (Figure 5B). For large vesicle ~76 nm in size, our simulation showed a dual-peak event that had also been observed in real recordings (Figure 5C). Based on our EM data (Figure 2B), vesicles with a diameter larger than ~65 nm occupied the upper 2.8.% of total synaptic vesicles, which was close to the detected 2.6.% of dual-peak events in the resting condition. Although other possibilities such as multi-vesicular release could also induce dual-peak events, most of them have only been reported in stimulated conditions (11, 12). Therefore, our simulations provided an alternative explanation in the resting condition.

4.6. Simulations of calcium/synaptotagmin-2 triggered exocytosis

Neurotransmitter release depends heavily on extracellular calcium concentration, which determines the amount of calcium influx upon stimulation (36, 37). To test the effect of calcium on mEPSCs, we applied 5 mM $CaCl_2$ in the bath solution and recorded mEPSCs after 3 min. Additional calcium increased the mEPSC frequency from 1.2. ± 0.3. Hz to 1.9. ± 0.6. Hz, while slightly decreasing the mEPSC amplitude from 33.0. ± 2.0. pA to 29.2. ± 3.2. pA (1100 events in 2 mM and 1023 events in 5 mM, $p < 0.0.5$, n = 4, Figure 6A). Our results were consistent with the previous study in neocortical neurons, which suggested that the decrease in mEPSC amplitudes is caused by the reduced electrochemical gradient (38). However, when we increased the extracellular Ca^{2+} to 5 mM, the extracellular Na^+ was only reduced by 4.5. mM in order to keep the osmolarity constant, which is a minor effect compared to the total 133 mM extracellular Na^+ in the control. It is very difficult to imagine that this would cause a ~20% decrease in mEPSC amplitude. Indeed,

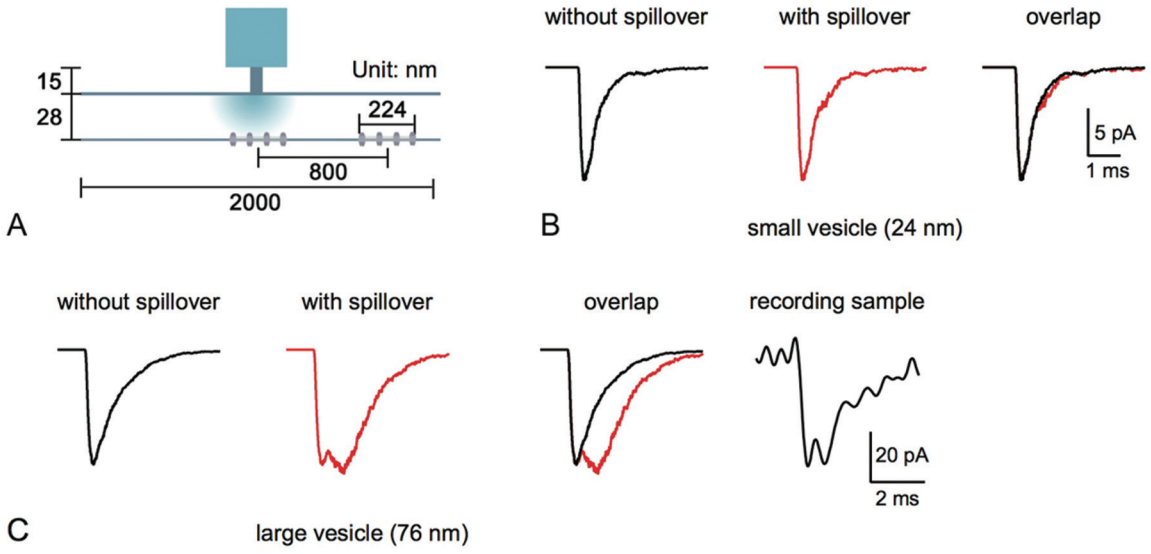

Figure 5. The contribution of glutamate spillover. (A) 2D cartoon showing neurotransmitter spillover. (B) Simulated mEPSCs of small vesicles (~24 nm) with (red, middle) and without (black, left) glutamate spillover. Traces are also overlapped to show the minor effect of glutamate spillover (right). (C) Simulated mEPSCs of large vesicles (~76 nm) with (red, 2nd Figure from the left) and without (black, left) glutamate spillover. Traces are also overlapped to show the dual peak effect of glutamate spillover (3rd Figure from the left). A trace from real recordings with dual peak is shown for comparison (right).

our scattered rise time distribution and cumulative probability curve showed an increased fraction of slower events after 5 mM calcium perfusion (Figures. 6B, C, $p < 0.0.1$, K-S test). The increased fraction of slower events suggests more kiss-and-run events based on our simulations. This result was consistent with a previous study indicating that high calcium shifts the exocytosis mode to kiss-and-run (39). Although compound vesicle fusion has been observed at the calyx of Held, which could also increase the rise time (11, 12), the reduced average mEPSC amplitude ruled out this possibility. Thus, we concluded that, with high extracellular calcium, the vesicles would undergo more kiss-and-run fusion, causing the increased fraction of slower rise time.

Synaptotagmins are the calcium sensors regulating exocytosis in nervous and endocrine systems (11, 26, 40). Calcium triggers vesicle release via binding to synaptotagmin, and at the calyx of Held the most abundant isoform of synaptotagmin is synaptotagmin-2. A previous study showed that, in *syt2* knock-out mice, the synchronous release is blocked, causing an increase in mEPSC frequency (26). However, whether *syt2* also regulates the vesicle fusion kinetics is not well studied. We explored this question by comparing the mEPSCs in $syt2^{+/+}$ and $syt2^{-/-}$ mice. Because the $syt2^{-/-}$ mice had a high frequency of spontaneous release, all mEPSCs were collected without Rs compensation. Two thousand events from both $syt2^{+/+}$ and $syt2^{-/-}$ mice were randomly selected for comparison. In $syt2^{+/+}$ mice, the mEPSC frequency was normal (1.0. ± 0.4. Hz, n = 5) with a mean amplitude of 27.4. ± 1.3. pA (Figure 6D, upper). The $syt2^{-/-}$ mEPSCs had a high frequency (12.1. ± 0.7. Hz) with similar amplitude (Figure 6D, lower, 26.9. ± 1.4. pA, n = 3, $p > 0.4$.). The scattered rise time distribution showed an apparent slowing down in the knock-out mice (Figure 6E). For example, for the fastest events located at the bottom of the distribution, the mEPSCs of $syt2^{-/-}$ mice had a steeper slope (slope: 1.3. $\mu s \cdot pA^{-1}$ in $syt2^{+/+}$ mice and 4.0. $\mu s \cdot pA^{-1}$ in $syt2^{-/-}$ mice). The cumulative probability curve of the $syt2^{-/-}$ mice also shifted to the right, suggesting more events with slower rise time (Figure 6F). Compound vesicle fusion was reported to be absent in $syt2^{-/-}$ mice (11) and we also did not observe an increase in amplitude. Therefore, in $syt2^{-/-}$ mice, the global slowing down in fusion kinetics may induce more kiss-and-run events, which was also consistent with our simulation results (Figure 6F). Synaptotagmin-1 has been suggested to stabilize the fusion pore before dilation (41) and promote fusion pore expansion (42). Our results confirmed that *syt2* also facilitated fusion pore dilation after the initial fusion pore opening in calyx-type synapses.

5. DISCUSSION

To better understand the vesicle fusion kinetics, we rebuilt the quantal release and its postsynaptic response by a three-dimensional model based on the Monte Carlo algorithm with updated parameters (4). By combining the simulation with mEPSCs collected from real recordings, our findings could be summarized in four points. First, at the presynaptic side, our simulations confirm that fusion pore opening kinetics and quantal

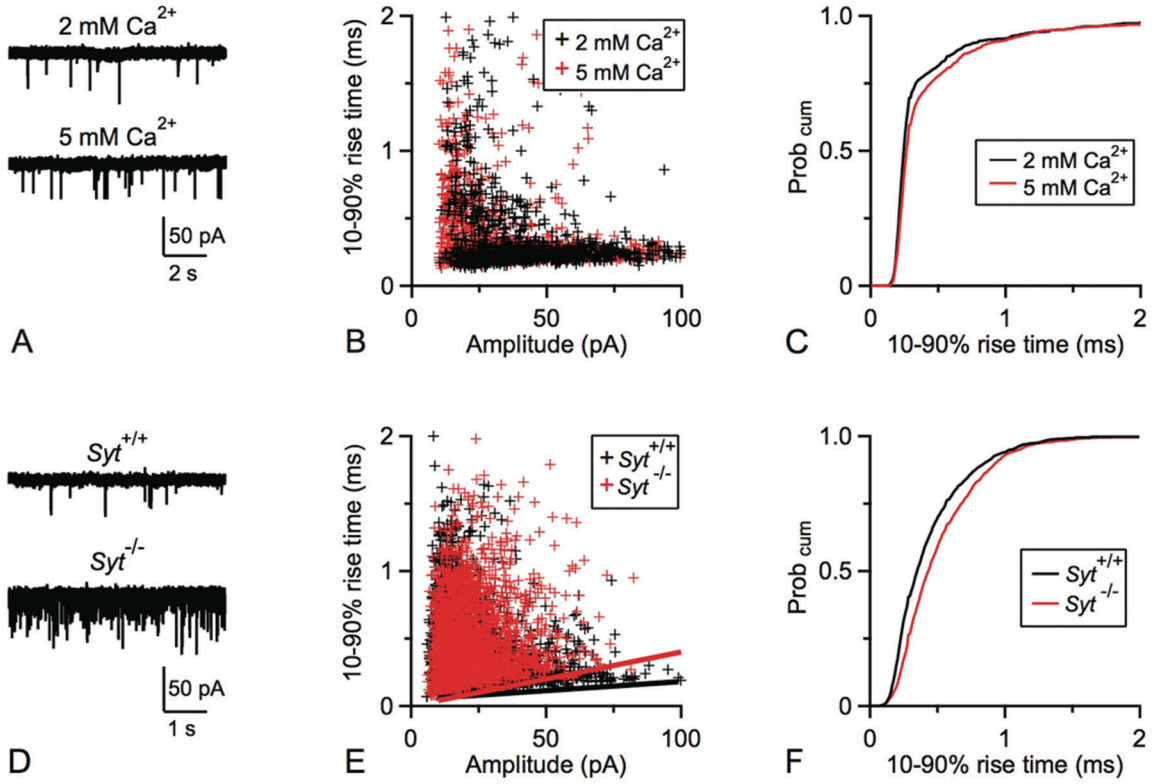

Figure 6. Calcium and synaptotagmin-2 regulated quantal release. (A) Sampled mEPSC recordings in bath solution containing 2 mM (upper) or 5 mM (lower) CaCl2. (B-C) The distribution and cumulative probability curve of mEPSCs with 2 mM (black) and 5 mM (red) CaCl2 in bath solution. (D) Sampled mEPSC recordings from wild-type (upper) and synaptotagmin-2 knock-out (lower) mice.(E-F) The distribution and cumulative probability curve of mEPSCs in wild-type (black) and synaptotagmin-2 knock-out (red) mice. The linear lines in (E) show the fit of fastest events in wild-type (black) and knock-out (red) mice.

size are the two major factors regulating postsynaptic currents. A previous study showed that only 3% of kiss-and-run fusion with Gp <288 pS could be detected in the KCl stimulation. Our estimation of kiss-and-run fusion based on simulations also confirmed this value, and we further suggest that the fraction of kiss-and-run is higher (12.4.%) in the resting condition which could not be detected in cell-attached recording because of the low frequency (8). In our study, the 10-90% rise time shifted to the left after KCl stimulation (Figure 3D), which suggests kiss-and-run with different initial fusion pore conductance under resting and stimulated conditions. Our results are in accordance with the conclusion from peptidergic vesicles, which indicates that stimulation reduces the fraction of smallest fusion pores (33).

Second, our recordings and simulations suggest that the location of the postsynaptic receptor cluster contributes to the huge deviation in mEPSC rise time. Although kiss-and-run and full fusion could account for the fastest and slowest fraction of mEPSCs in our recordings, a large number events still occur in between. Previous studies have suggested that multi-vesicular release may account for the high variability at different synapses (43, 44), but in the resting condition, multi-vesicular release has been shown to be minimal at calyces (8). Our results suggest a possible role from the postsynaptic side: the variations in distance between AMPA receptor clusters and the release site account for the variation in mEPSC rise time.

Third, calcium influx triggers exocytosis (37, 45). In additional to regulating the number of vesicles being released (46), calcium has also been reported to influence fusion pore kinetics (39, 41). We evaluated how calcium regulates vesicle fusion kinetics in our study. Surprisingly, with the exception of increased mEPSC frequency (Figure 6A), calcium did not facilitate vesicle fusion, as reflected in the lack of a further decrease in rise time. However, we also observed reduced mEPSC amplitude and more slow events, which suggest that calcium increased the fraction of kiss-and-run events. A previous study using amperometric recordings at chromaffin cells reported that high calcium shifts the exocytosis mode to kiss-and-run (39). Our results suggest a similar mechanism for calcium in changing the vesicle fusion mode at calyx-type synapses.

Fourth, synaptotagmins are not only calcium sensors that trigger calcium dependent exocytosis (40, 47, 48), they also have been shown to play a critical role in the regulation of fusion pore kinetics (41, 49), determining the fate of different fusion modes. Although calcium triggers exocytosis by binding to synaptotagmin, calcium and synaptotagmin may influence fusion kinetics in different ways (40). A recent *in vitro* study showed that synaptotagmin-1 can promote calcium triggered fusion pore expansion (42), but how synaptotagmin-2 regulates fusion pore opening and dilation at calyces remains unknown. We showed a slowing down of fusion kinetics in synaptotagmin-2 knock-out mice, which may induce more kiss-and-run events (Figures. 6E, F). Our results are consistent with previous studies showing that synaptotagmin regulates fusion pore stability (41, 49-51).

In summary, using 3D Monte Carlo simulation of quantal release, the present study demonstrates a very useful tool for mimicking the details of vesicle fusion at the release site, which is quite difficult for technically approaching for a long time. Our model clearly shows how vesicle fusion is regulated by major presynaptic and postsynaptic sources by comparing mEPSC amplitudes and rise time. Though difficult techniques such as cell-attached recording, have been used to verify different fusion modes from release sites (7, 8, 11) in the past decade, our model provides a convenient method for looking into fusion events merely by checking the postsynaptic mEPSCs, which mirror the fusion pore kinetics of the postsynaptic membrane.

6. ACKNOWLEDGEMENT

This work was sponsored by Shanghai Pujiang Program, National Natural Science Foundation of China (grant number: 31370828) and Specialized Research Fund for the Doctoral Program of Higher Education (SRFDPF, grant number: 20120071120013) and the Shanghai Leading Academic Discipline Project (B111).

7. REFERENCES

1. R. D. Burgoyne and J. W. Barclay: Splitting the quantum: regulation of quantal release during vesicle fusion. *Trends in Neurosciences*, 25(4), 176-178 (2002)
DOI: 10.1016/S0166-2236(00)02126-3

2. J. G. Borst and J. Soria van Hoeve: The calyx of held synapse: from model synapse to auditory relay. *Annu Rev Physiol*, 74, 199-224 (2012)
DOI: 10.1146/annurev-physiol-020911-153236

3. X. S. Wu, L. Xue, R. Mohan, K. Paradiso, K. D. Gillis and L. G. Wu: The origin of quantal size variation: vesicular glutamate concentration plays a significant role. *J Neurosci*, 27(11), 3046-3056 (2007)
DOI: 10.1523/JNEUROSCI.4415-06.2007

4. T. Budisantoso, H. Harada, N. Kamasawa, Y. Fukazawa, R. Shigemoto and K. Matsui: Evaluation of glutamate concentration transient in the synaptic cleft of the rat calyx of Held. *J Physiol*, 591(Pt 1), 219-39 (2013)
DOI: 10.1113/jphysiol.2012.241398

5. d. T. Alvarez, R. Fernandez-Chacon and J. M. Fernandez: Release of secretory products during transient vesicle fusion. *Nature*, 363(6429), 554-558 (1993)
DOI: 10.1038/363554a0

6. R. Fesce, F. Grohovaz, F. Valtorta and J. Meldolesi: Neurotransmitter release, fusion or 'kiss and run'? *Trends in Cell Biology*, 4, 1-4 (1994)
DOI: 10.1016/0962-8924(94)90025-6

7. V. A. Klyachko and M. B. Jackson: Capacitance steps and fusion pores of small and large-dense-core vesicles in nerve terminals. *Nature*, 418, 89-92 (2002)
DOI: 10.1038/nature00852

8. L. He, X. S. Wu, R. Mohan and L. G. Wu: Two modes of fusion pore opening revealed by cell-attached recordings at a synapse. *Nature*, 444(7115), 102-105 (2006)
DOI: 10.1038/nature05250

9. D. Zenisek, J. A. Steyer, M. E. Feldman and W. Almers: A membrane marker leaves synaptic vesicles in milliseconds after exocytosis in retinal bipolar cells. *Neuron*, 35(6), 1085-1097 (2002)
DOI: 10.1016/S0896-6273(02)00896-6

10. Q. Zhang, Y. Li and R. W. Tsien: The dynamic control of kiss-and-run and vesicular reuse probed with single nanoparticles. *Science*, 323(5920), 1448-53 (2009)
DOI: 10.1126/science.1167373

11. L. He, L. Xue, J. Xu, B. D. McNeil, L. Bai, E. Melicoff, R. Adachi and L. G. Wu: Compound vesicle fusion increases quantal size and potentiates synaptic transmission. *Nature*, 459(7243), 93-7 (2009)
DOI: 10.1038/nature07860

12. J. H. Singer, L. Lassova, N. Vardi and J. S. Diamond: Coordinated multivesicular release at a mammalian ribbon synapse. *Nat. Neurosci*, 7(8), 826-833 (2004)
DOI: 10.1038/nn1280

13. S. Karunanithi, L. Marin, K. Wong and H. L. Atwood: Quantal size and variation determined by vesicle size in normal and mutant Drosophila glutamatergic synapses. *J.Neurosci.*, 22(23), 10267-10276 (2002)
No DOI found

14. K. Sätzler, L. Sohl, J. H. Bollmann, J. G. G. Borst, M. Frotscher, B. Sakmann and J. H. Lubke: Three-dimensional reconstruction of a calyx of Held and its postsynaptic principal neuron in the medial nucleus of the trapezoid body. *J Neurosci*, 22, 10567-10579 (2002)
No DOI found

15. N. Riveros, J. Fiedler, N. Lagos, C. Munoz and F. Orrego: Glutamate in rat brain cortex synaptic vesicles: influence of the vesicle isolation procedure. *Brain Res*, 386(1-2), 405-8 (1986)
DOI: 10.1016/0006-8993(86)90181-2

16. P. M. Burger, E. Mehl, P. L. Cameron, P. R. Maycox, M. Baumert, F. Lottspeich, P. De Camilli and R. Jahn: Synaptic vesicles immunoisolated from rat cerebral cortex contain high levels of glutamate. *Neuron*, 3(6), 715-20 (1989)
DOI: 10.1016/0896-6273(89)90240-7

17. G. A. Zampighi and R. S. Fisher: Polyhedral protein cages encase synaptic vesicles and participate in their attachment to the active zone. *J Struct Biol*, 119(3), 347-59 (1997)
DOI: 10.1006/jsbi.1997.3882

18. S. Takamori, M. Holt, K. Stenius, E. A. Lemke, M. Gronborg, D. Riedel, H. Urlaub, S. Schenck, B. Brugger, P. Ringler, S. A. Muller, B. Rammner, F. Grater, J. S. Hub, B. L. De Groot, G. Mieskes, Y. Moriyama, J. Klingauf, H. Grubmuller, J. Heuser, F. Wieland and R. Jahn: Molecular anatomy of a trafficking organelle. *Cell*, 127(4), 831-846 (2006)
DOI: 10.1016/j.cell.2006.10.030

19. K. M. Franks, C. F. Stevens and T. J. Sejnowski: Independent sources of quantal variability at single glutamatergic synapses. *J.Neurosci.*, 23(8), 3186-3195 (2003)
No DOI found

20. L. Cathala, N. B. Holderith, Z. Nusser, D. A. Digregorio and S. G. Cull-Candy: Changes in synaptic structure underlie the developmental speeding of AMPA receptor-mediated EPSCs. *Nat.Neurosci*, 8(10), 1310-1318 (2005)
No DOI found

21. J. S. Diamond: Neuronal glutamate transporters limit activation of NMDA receptors by neurotransmitter spillover on CA1 pyramidal cells. *J Neurosci*, 21(21), 8328-38 (2001)
No DOI found

22. K. Matsui and C. E. Jahr: Ectopic release of synaptic vesicles. *Neuron*, 40(6), 1173-1183 (2003)
DOI: 10.1016/S0896-6273(03)00788-8

23. M. A. Xu-Friedman and W. G. Regehr: Ultrastructural contributions to desensitization at cerebellar mossy fiber to granule cell synapses. *J Neurosci*, 23(6), 2182-92 (2003)
No DOI found

24. J. S. Coggan, T. M. Bartol, E. Esquenazi, J. R. Stiles, S. Lamont, M. E. Martone, D. K. Berg, M. H. Ellisman and T. J. Sejnowski: Evidence for ectopic neurotransmission at a neuronal synapse. *Science*, 309(5733), 446-451 (2005)
DOI: 10.1126/science.1108239

25. J. R. Stiles, T. B. bartol, M. M. Salpeter, E. E. Salpeter and T. J. Sejnowski: Synaptic variability. In: *Synapses*. Ed T. C. Cowan, T. C. Sudhof&C. F. Stevens. The Johns Hopkins University Press, Baltimore (2000)
No DOI found

26. J. Sun, Z. P. Pang, D. Qin, A. T. Fahim, R. Adachi and T. C. Sudhof: A dual-Ca2+-sensor model for neurotransmitter release in a central synapse. *Nature*, 450(7170), 676-82 (2007)
DOI: 10.1038/nature06308

27. Z. P. Pang, J. Sun, J. Rizo, A. Maximov and T. C. Sudhof: Genetic analysis of synaptotagmin 2 in spontaneous and Ca2+-triggered neurotransmitter release. *EMBO J*, 25(10), 2039-2050 (2006)
DOI: 10.1038/sj.emboj.7601103

28. D. Bruns, D. Riedel, J. Klingauf and R. Jahn: Quantal release of serotonin. *Neuron*, 28(1), 205-220 (2000)
DOI: 10.1016/S0896-6273(00)00097-0

29. A. E. Spruce, L. J. Breckenridge, A. K. Lee and W. Almers: Properties of the fusion pore that forms during exocytosis of a mast cell secretory vesicle. *Neuron*, 4(5), 643-654 (1990)
DOI: 10.1016/0896-6273(90)90192-I

30. T. A. Nielsen, D. A. Digregorio and R. A. Silver: Modulation of glutamate mobility reveals the mechanism underlying slow-rising AMPAR

EPSCs and the diffusion coefficient in the synaptic cleft. *Neuron*, 42(5), 757-771 (2004) DOI: 10.1016/j.neuron.2004.04.003

31. S. Choi, J. Klingauf and R. W. Tsien: Fusion pore modulation as a presynaptic mechanism contributing to expression of long-term potentiation. *Philos.Trans.R.Soc.Lond B Biol. Sci.*, 358(1432), 695-705 (2003) DOI: 10.1098/rstb.2002.1249
32. Y. Sahara and T. Takahashi: Quantal components of the excitatory postsynaptic currents at a rat central auditory synapse. *J Physiol*, 536(Pt 1), 189-197 (2001) DOI: 10.1111/j.1469-7793.2001.00189.x
33. N. Vardjan, M. Stenovec, J. Jorgacevski, M. Kreft and R. Zorec: Subnanometer fusion pores in spontaneous exocytosis of peptidergic vesicles. *J Neurosci*, 27(17), 4737-46 (2007) DOI: 10.1523/JNEUROSCI.0351-07.2007
34. T. Ishikawa, Y. Sahara and T. Takahashi: A single packet of transmitter does not saturate postsynaptic glutamate receptors. *Neuron*, 34(4), 613-621 (2002) DOI: 10.1016/S0896-6273(02)00692-X
35. D. A. Digregorio, Z. Nusser and R. A. Silver: Spillover of glutamate onto synaptic AMPA receptors enhances fast transmission at a cerebellar synapse. *Neuron*, 35(3), 521-533 (2002) DOI: 10.1016/S0896-6273(02)00787-0
36. F. A. Dodge, R. Miledi and R. Rahamimoff: Strontium and quantal release of transmitter at the neuromuscular junction. *J.Physiol.*, 200, 267-283 (1969) No DOI found
37. L. G. Wu, R. E. Westenbroek, J. G. G. Borst, W. A. Catterall and B. Sakmann: Calcium channel types with distinct presynaptic localization couple differentially to transmitter release in single calyx-type synapses. *J.Neuorsci.*, 19, 726-736 (1999) No DOI found
38. N. P. Vyleta and S. M. Smith: Spontaneous glutamate release is independent of calcium influx and tonically activated by the calcium-sensing receptor. *J Neurosci*, 31(12), 4593-606 (2011) DOI: 10.1523/JNEUROSCI.6398-10.2011
39. E. Ales, L. Tabares, J. M. Poyato, V. Valero, M. Lindau and G. Alvarez de Toledo: High calcium concentrations shift the mode of exocytosis to the kiss-and-run mechanism. *Nat Cell Biol*, 1(1), 40-4 (1999) No DOI found
40. P. K. Moghadam and M. B. Jackson: The functional significance of synaptotagmin diversity in neuroendocrine secretion. *Front Endocrinol (Lausanne)*, 4, 124 (2013) No DOI found
41. C. T. Wang, J. Bai, P. Y. Chang, E. R. Chapman and M. B. Jackson: Synaptotagmin-Ca^{2+} triggers two sequential steps in regulated exocytosis in rat PC12 cells: fusion pore opening and fusion pore dilation. *J Physiol*, 570(Pt 2), 295-307 (2006) No DOI found
42. Y. Lai, J. Diao, Y. Liu, Y. Ishitsuka, Z. Su, K. Schulten, T. Ha and Y. K. Shin: Fusion pore formation and expansion induced by Ca^{2+} and synaptotagmin 1. *Proc Natl Acad Sci U S A*, 110(4), 1333-8 (2013) DOI: 10.1073/pnas.1218818110
43. M. J. Wall and M. M. Usowicz: Development of the quantal properties of evoked and spontaneous synaptic currents at a brain synapse. *Nat.Neurosci*, 1(8), 675-682 (1998) DOI: 10.1038/3677
44. S. Raghavachari and J. E. Lisman: Properties of quantal transmission at CA1 synapses. *J Neurophysiol*, 92(4), 2456-67 (2004) DOI: 10.1152/jn.00258.2004
45. G. J. Augustine: How does calcium trigger neurotransmitter release? *Curr Opin Neurobiol*, 11(3), 320-6 (2001) DOI: 10.1016/S0959-4388(00)00214-2
46. L. G. Wu and P. Saggau: Presynaptic inhibition of elicited neurotransmitter release. *Trends in neuroscience*, 20, 204-212 (1997) DOI: 10.1016/S0166-2236(96)01015-6
47. N. Brose, A. G. Petrenko, T. C. Sudhof and R. Jahn: Synaptotagmin:a calcium sensor on the synaptic vesicle surface. *Science*, 256, 1021-1025 (1992) DOI: 10.1126/science.1589771
48. E. R. Chapman: How does synaptotagmin trigger neurotransmitter release? *Annu Rev Biochem*, 77, 615-41 (2008) DOI: 10.1146/annurev.biochem.77.062005.101135

49. J. Bai, C. T. Wang, D. A. Richards, M. B. Jackson and E. R. Chapman: Fusion pore dynamics are regulated by synaptotagmin*t-SNARE interactions. *Neuron*, 41(6), 929-42 (2004)
DOI: 10.1016/S0896-6273(04)00117-5

50. C. T. Wang, J. C. Lu, J. Bai, P. Y. Chang, T. F. Martin, E. R. Chapman and M. B. Jackson: Different domains of synaptotagmin control the choice between kiss-and-run and full fusion. *Nature*, 424(6951), 943-947 (2003)
DOI: 10.1038/nature01857

51. Z. Zhang, E. Hui, E. R. Chapman and M. B. Jackson: Regulation of exocytosis and fusion pores by synaptotagmin-effector interactions. *Mol Biol Cell*, 21(16), 2821-31 (2010)
DOI: 10.1091/mbc.E10-04-0285

Abbreviation: mEPSC: miniature excitatory postsynaptic current; AMPA: α-amino-3-hydroxy-5-methyl-4-isoxazole-propionic acid; EM: electron microscopy

Key Words: Quantal Release, Fusion Pore, Mcell, Synaptotagmin

Send correspondence to: Lei Xue, Room D213, Life Sciences Building, Jiangwan Campus, Fudan University, Shanghai, 200433, Tel: 86-21-51630392, Fax: 86-21-51630392, E-mail: lxue@fudan.edu.cn